Propagation of sound beams behind sonic crystals

V. J. Sánchez-Morcillo,[1] K. Staliunas,[2] V. Espinosa,[1] I. Pérez-Arjona,[1] J. Redondo,[1] and E. Soliveres[1]
[1]*Instituto de Investigación para la Gestión Integrada de Zonas Costeras, Universidad Politécnica de Valencia, Carretera Natzaret-Oliva, s/n 46730 Grao de Gandia, Spain*
[2]*ICREA, Departament de Fisica i Enginyeria Nuclear, Universitat Politècnica de Catalunya, Colom, 11, E-08222 Terrassa, Barcelona, Spain*
(Received 24 February 2009; published 20 October 2009)

A theoretical and experimental study of the propagation of sound beams in and behind two-dimensional sonic crystals at frequencies close to the band edges is presented. Beam focusing is predicted and discussed. We evaluate, by analytical numerical methods, the main focusing characteristics, such as the focal distance, the width of beam waist, and the beam quality at the waist. The field distribution is shown to depend strongly on the beam size and frequency. Experiments were performed on narrow sources radiating in ultrasound regime, although the results are extendable to arbitrary frequencies.

DOI: 10.1103/PhysRevB.80.134303 PACS number(s): 63.20.−e, 43.35.+d

I. INTRODUCTION

The spatially modulated materials, also known as sonic crystals (SCs) in acoustics or photonic crystals (PCs) in optics, are famous mostly due to their celebrate temporal dispersion properties, in particular, due to the appearance of band gaps in the dispersion curves (see Ref. 1 for photonic band gaps in optics and Ref. 2 for phononic band gaps in acoustics). We are reminded that the temporal dispersion is the frequency dependence on the propagation wave number $\omega=\omega(|\mathbf{k}|)$, where in a two-dimensional (2D) geometry, the wave vector $\mathbf{k}=(k_{\parallel},k_{\perp})$ is defined by its parallel and perpendicular components with respect to the propagation direction. In addition to the peculiarities of temporal dispersion, the spatially modulated materials are known also to modify the spatial dispersion (also called diffraction), allowing the managing of the diffractive broadening of the beams. This phenomenon is usually interpreted in terms of the spatial dispersion diagrams, given by the curves of constant frequency in $\vec{k}$ space, i.e., $k_{\parallel}=k_{\parallel}(k_{\perp})$, which in paraxial optics are called "diffraction" curves. The peculiarities of the spatial dispersion in periodic materials can result in subdiffraction or self-collimation, reported both in optics[3] and in acoustics.[4,5] Self-collimation is related with the appearance of flat segments in the spatial dispersion curve and results in nondiffractive propagation of the beams and wave patterns. The modification of the spatial dispersion can also lead to the superrefraction, and to the lensing and superlensing (subwavelength focusing), of light[6] and of sound,[7] when strongly tilted, or strongly curved segments in the dispersion curves appear. There are a number of previous works which have considered the negative refraction[8–10] and the focusing properties of 2D (Refs. 11–16) and three-dimensional[17] sonic crystals.

The effects of lensing and superlensing are, however, often treated inconsistently in optics, as well as in acoustics. Usually the band diagrams and the spatial dispersion curves (isolines of frequency) are first calculated, based on the Bloch-wave theory (harmonic expansion). Then, depending on the slopes of the spatial dispersion curves the effective refraction index is phenomenologically introduced. Based on the refraction index the geometric ray approach is often applied and the images of the point sources are calculated.

This approach, which mixes the concepts of the wave mechanics and the geometrical ray propagation, often leads to inconsistent and confusing results. For example, the focal distance resulting from a slice of the focusing PC or SC (the PC or SC lens) should decrease by approaching the band gaps, as the curvatures of the spatial dispersion curves increase and, consequently, the strength of the "lenses" increases, according to this mixed wave-ray approach. We, however, by following consistently the solely wave approach, show the opposite effect: as the wave frequency approaches the band-gap frequency, the focal distance of the SC lens increases, not decreases.

Therefore it seems that some clarity must be brought into the problem of the lensing effects in PC or SC materials. The paper aims to clarify the questions related with the focusing of sound beams behind the sonic crystal. In this way, differently from the previous "superlensing" studies, we consider the propagation and collimation of beams with finite size, not the focusing of the waves emitted by the point sources.

The paper is organized in the following way. In Sec. II A the model is introduced and in Sec. II B the band diagrams (isofrequency contours) are evaluated for a concrete case. Based on the band diagram structure, in Sec. II C several models for beam propagation, of increasing complexity, are proposed. Next in Sec. III we proceed with the analytical estimations following from these models. In particular, we calculate the focal distances, the beamwidth and the quality of the beam at the waist (in the focal spot behind the SC). In this section these evaluations are checked by the numerical finite difference in time domain (FDTD) calculations. In Sec. IV experimental setup and the measurements of the field distributions beyond the crystal for a narrow beam are presented and compared with the previous theory. Finally, Sec. V represents the conclusions.

II. THEORY

A. Model

The propagation of a sound beam in a spatially modulated medium is described by the inhomogeneous wave equation

$$\frac{1}{B(\mathbf{r})}\frac{\partial^2 p(\mathbf{r},t)}{\partial t^2} + \nabla\left[\frac{1}{\rho(\mathbf{r})}\nabla p(\mathbf{r},t)\right] = 0, \tag{1}$$

where the functions $B(\mathbf{r})$ and $\rho(\mathbf{r})$ are, respectively, the spatially dependent (periodic) bulk modulus and density of the periodic medium, and $p(\mathbf{r},t)$ is the scalar pressure field of the sound wave. As we restrict the analysis to that of a monochromatic wave with frequency ω, then $p(\mathbf{r},t) = p(\mathbf{r})\exp(i\omega t)$ and the problem reduces to the time-independent eigenvalue equation

$$\frac{\omega^2}{B(\mathbf{r})}p(\mathbf{r}) + \nabla\left[\frac{1}{\rho(\mathbf{r})}\nabla p(\mathbf{r})\right] = 0, \tag{2}$$

which will be used to build the band diagrams.

We start our analysis by considering a family of spatial dispersion curves for a 2D sonic crystal, obtained by solving Eq. (2) by the harmonic expansion method. In the numerical study, and also in the experiments described in the next section, we consider a sonic crystal of the square geometry, consisting of a periodic array of steel cylinders with radius $r=0.8$ mm and lattice constant $a=5.25$ mm, as, e.g., in Ref. 5, resulting in a filling factor $f=\pi(r/a)^2=0.073$. The material parameters are $\rho_h=10^3$ Kg m^{-3} and $B_h=2.2\times10^9$ N m^{-2} for the host medium (water) and $\rho_s=7.8\times10^3$ Kg m^{-3} and $B_s=160\times10^9$ N m^{-2} for steel, with corresponding sound velocities $c_h=1483$ m s^{-1} and $c_s=4530$ m s^{-1}. In such a crystal, the frequencies of interest correspond to the ultrasonic regime. The results presented in the following sections are however rescalable and valid for arbitrary frequency ranges.

B. Band diagrams

In Fig. 1 the isofrequency contours from the first two lowest bands are shown, combined into one plot, for convenience. As usual, normalized frequency and wave number are used, defined as $\Omega=\omega a/2\pi c_h$ and $K=ka/2\pi$. We consider frequencies close to the first and second band gaps (the band gaps are centered at $\Omega=1/\sqrt{2}$ and $\Omega=1$), and corresponding to the symmetry points M and Γ in the first and second Brillouin zones, respectively. The shaded triangles denote the incident beams.

Figure 1 illustrates several things. On one hand it shows the frequencies of interest, where focusing is expected to occur. These regimes are close to the upper boundaries of the bands, where the dispersion curves are convex (corresponding to the negative diffraction regime). The curvatures of the dispersion curves at the areas of interest are positive, in contrast to the curves with negative curvature at lower frequencies indicating the normal diffraction. Only in this case of positive curvatures (negative diffraction) of the SC, the focusing of the beams behind the crystal is possible. Figure 1(a) also shows the equivalence of the focusing effects at both the first and the second band edges, as the corresponding isofrequency lines can be obtained one from another by rotation by 45° and by a rescaling of the wave vectors and the frequency in a factor $\sqrt{2}$. These two band gaps were already studied from the unified point of view in Ref. 4.

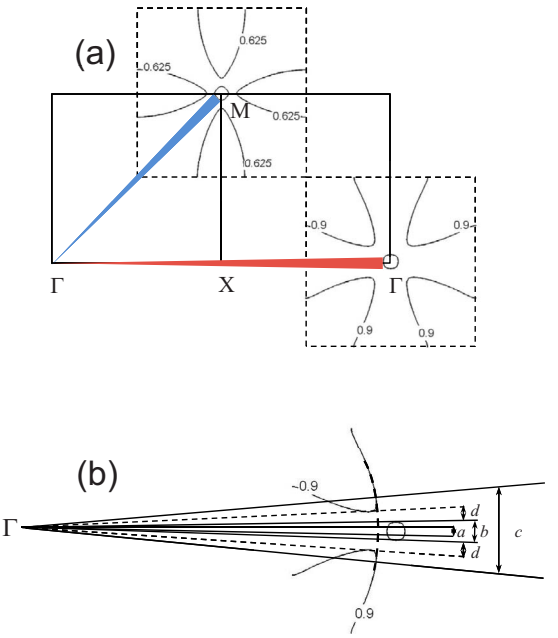

FIG. 1. (Color online) (a) The spatial dispersion curves as calculated by the harmonic expansion (see Ref. 4 for details of the method). The thick curves represent the areas considered, i.e., are calculated for wave frequencies close to the upper boundaries of the first and second bands. Shaded triangles (red and blue curves) denote the spatial angular spectrum incident of the incident beams. (b) Different regimes considered: (a) broad beams with spatial spectra inside the "parabolic" area of the spatial dispersion curve, (b) beams of intermediate width, with spatial spectra filling the full width of the isoline of the given band, (c) narrow beams with the spatial spectra extending over isolines from the neighboring bands, and thus overlapping the band gaps (in angular domain). The region denoted by (d) corresponds to the forbidden angles (band gaps in space spectra domain).

C. Regimes

However, most importantly, Fig. 1(b) also shows the possibility of three different focusing regimes by a SC, depending on the beam size: (a) ideal (or aberration-free) focusing of relatively broad beams (those with a sufficiently narrow spatial spectrum). We recall that spatial and angular (spectral) distributions are related via the Fourier transform. In general terms, the wider the spatial beamwidth, the narrower its spatial spectrum. The regime (a) occurs when the spectrum is so narrow that the corresponding segment of the spatial dispersion curve can be considered parabolic [the segment labeled by *a* in Fig. 1(b)]; (b) focusing with aberrations, when the spatial spectrum of the beam becomes broader (the beam becomes narrower) and projects on all the dispersion curve of the particular band [segment *b* in Fig. 1(b)]. The aberration effects come into play in the latter case, as the corresponding area of the spatial dispersion profile is characterized no more by parabolic dispersion but also by higher order effects (nonparabolic part of the spatial dispersion curve); and (c) a focusing with a significant distortion of the spatial spectrum of the beam and consequently with a decrease in the beam quality, when the spatial spectrum becomes significantly broader than the central area of the dis-

persion curve. The focusing in the latter limit is also affected by the spatial dispersion curves belonging to the neighboring band (segment *c*). The segment denoted by *d* corresponds to a gap in the spatial spectrum domain and the spatial frequencies lying on this segment are removed (filtered out) from the beam as it propagates through the crystal.

We note that the width of the spatial spectrum of the beam has a sense in comparison to the width of the loop of the spatial dispersion curve. Close to the band gap, where the spatial dispersion loop shrinks, the limiting width of the beam (separating broad and narrow beam regimes) increases. We consider this issue below.

In order to illustrate the existence of the three different focusing regimes, numerical calculations have been performed by solving Eq. (1) using the FDTD technique (see details, e.g., in Ref. 4) with input beams of different width. We assume infinite impedance of the cylinders and consequently neglect shear wave propagation in the scatterers. Figure 2 shows the resulting pressure distribution for a beam with constant frequency of 230 kHz and a decreasing width, relative to the lattice period, of $L/a=8$, 4, and 2, respectively. We observe behaviors corresponding to cases (a)–(c) discussed above and illustrated in Fig. 1(b).

III. ANALYTIC ESTIMATIONS

We proceed to the study of the beam propagation characteristics, corresponding to the three basic regimes identified above. In analytical-conceptual treatment we use the following approach. First we calculate the band structure of the sonic crystal using the standard approach of the plane-wave expansion method: we consider the wave equation [Eq. (1)] with spatially periodic coefficients, expand the fields in the harmonic components, diagonalize the resulting coupled equation system (find the Bloch modes), and calculate the eigenvalues of frequency. Then we use, as described in Ref. 4, the analytical estimations of the spectral width of the propagation area (corresponding to the band studied), as well as the curvatures (second-order derivatives) and the astigmatisms (fourth-order derivatives) of the spatial dispersion curves. Finally, using the above data from the wave equation approach for the evaluation of the dispersion characteristics, we investigate the propagation properties of the beams in the simplified paraxial approximation, valid for beams forming small angles with respect to the axis. The results shown in Fig. 2 justify the validity of this approach for the considered problem.

The coefficients of diffraction (of the leading-order diffraction, i.e., the usual diffraction, as well as of the higher order diffraction terms) are determined by the shape of the spatial dispersion curves $K_\parallel=K_\parallel(K_\perp)$ and are found by its series expansion. Following,[4] they can be analytically estimated by assuming a small filling factor $f=\pi(r/a)^2\approx O(\varepsilon^2)$ and the close-to-band-gap condition $\Delta\Omega=(\Omega_g-\Omega)/\Omega_g \approx O(\varepsilon)$. Under these assumptions, $K_\parallel=K_\parallel(K_\perp)$ can be expanded as

$$K_\parallel = d_0 + d_2K_\perp^2 + d_4K_\perp^4 + \cdots, \tag{3}$$

where the coefficients are dependent on the beam and crystal parameters, through the frequency and the filing factor, respectively, and take the form

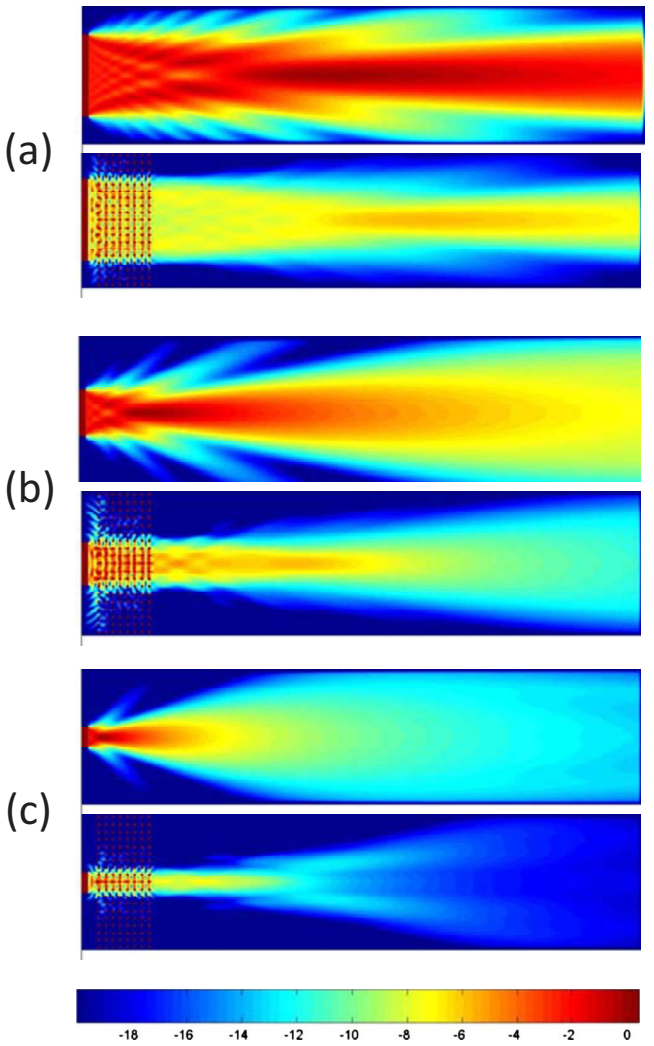

FIG. 2. (Color online) Numerically calculated beam profiles, showing the propagation inside and outside the crystal. Three cases (a), (b), and (c) correspond to three relatively different widths of the beams. Each figure shows the propagation with (bottom) and without (top) sonic crystal. The parameters are: (a) $D=8a$, (b) $D=4a$, and (c) $D=2a$, where D is the source diameter and a the lattice period. The frequency is 230 kHz in all three cases. Amplitudes are given in decibel scale. The size of the integration region is 40 $\times 10$ cm^2.

$$d_0 = \alpha\Delta\Omega + O(\varepsilon),$$

$$d_2 = \alpha\left(1 - \frac{f^2}{\Delta\Omega^3}\right) + O(\varepsilon),$$

$$d_4 = 2\alpha\left(\frac{1}{\Delta\Omega^2} - \frac{f^2}{\Delta\Omega^5}\right) + O(\varepsilon^{-1}), \tag{4}$$

where α is a geometrical factor that depends on the band number, being $\alpha=1/\sqrt{2}$ and $\alpha=1$ for the first and second bands, respectively. We recall that the detuning term $\Delta\Omega \geq 0$, where $\Delta\Omega=0$ denotes the middle of the band gap and corresponds to the triple cross section of the circular dispersion curves of harmonics, and $|\Delta\Omega_{ZDP}|=f^{2/3}$ corresponds to

the zero diffraction point (ZDP) where the diffraction coefficient d_2 vanishes.

In the paraxial treatment, the beam broadening after the propagation in a homogeneous material with diffraction coefficient d_2 is given by $\Delta x^2(z)=\Delta x_0^2+(4d_2z)^2/\Delta x_0^2$, where Δx_0 is the initial width. The above classical formula appears due to the parabolic form of the dispersion curve, which introduces the parabolic shape of the phase shift of the components of the spatial spectrum $\Delta\varphi(K_\perp)=-d_2K_\perp^2L$. In the normal diffraction regime $\Omega<\Omega_{\mathrm{ZDP}}$ the components with increasing angle to the optical axis $k_\perp$ obtain a negative phase shift. The propagation of the beam behind the crystal can only increase the negative phase shift already accumulated during the propagation through the SC. Therefore the propagation behind the SC is trivial: the beam simply expands. For $\Omega>\Omega_{\mathrm{ZDP}}$ the situation is different—the components with nonzero $K_\perp$ acquire the positive phase shift in the SC. Therefore in the propagation behind the SC, a homogeneous material can compensate this positive phase shift, i.e., can result in the collimation of the beam. We concentrate on the latter regime, and calculate how and where the beam focuses. In other words, the focusing behind the crystal is due to the fact that inside the SC the beam propagates with negative diffraction and acquires the negative curvature of the phase fronts. Therefore, the crystal acts as a focusing lens. As the result, the beam behind the SC focuses in a free propagation, at a variable distance which depends on both the crystal and source properties (width and frequency).

Next we present three focusing models to describe the different regimes of the beam propagation inside and outside the SC discussed above.

(1) Model A considers the case of broad Gaussian beams (narrow Gaussian spatial spectra) and assumes a parabolic (aberration-free) focusing. No distortion of the Gaussian beams due to higher order diffraction corrections is considered ($d_4K^4\to 0$). The results in the frame of the model are quite simple. (1) The width of the beam at the focal point is always the same as the width of the initial beam. This follows from the fact that the spectral width of the beam is unchanged during all the propagation. (2) The focal distance behind the crystal can be calculated considering that the spatial spectra components are again mutually in phase in focus. This means $d_2L+z_f=0$ (where L is the length of the SC) or in terms of the SC parameters

$$z_f=-\alpha L\left(1-\frac{f^2}{\Delta\Omega^3}\right). \tag{5}$$

Equation (5) implies that the focal distance vanishes at ZDP ($|\Delta\Omega_{\mathrm{ZDP}}|=f^{2/3}$) and increases monotonically to infinity at the band edge. Close to the band gap (in the limit $\Delta\Omega\to 0$) Eq. (3) takes the simplified form $z_f=\alpha Lf^2/|\Delta\Omega|^3$.

Figure 3(a) compares the numerical results for the focal distance obtained by solving Eq. (1) by the FDTD method with the analytical expression Eq. (5), derived under the paraxial approximation, for a beam propagating along the ⟨110⟩ direction. The frequencies belong to the first propagation band (similar results are obtained for the second band). Note a good agreement with the result following from FDTD calculations in the case of a broad (unfiltered) beam, in spite of the simplicity of the model and Eq. (5).

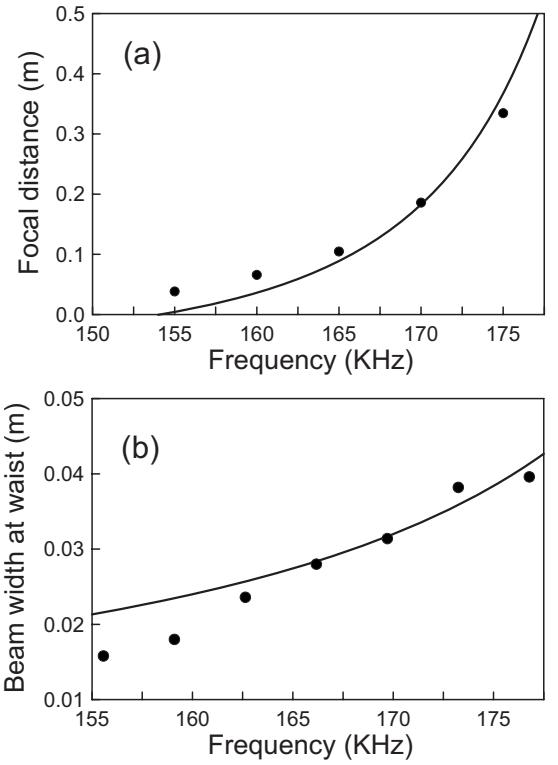

FIG. 3. (a) Focal distance of the sonic crystal lens for frequencies inside the first band, evaluated from the analytical expression Eq. (5) (continuous line) and by numerical simulation using the FDTD method (symbols). (b) Beamwidth at the focal distance, evaluated from Eq. (6), with the corresponding numerical result (symbols). A broad beam with $L=8a$ [case (a) in Fig. 2] is used as the input beam in (a) while $L=4a$ in (b). The parameters are $f=0.073$ and $L=0.1$ m.

(2) Model B is applicable for beams of intermediate width or equivalently, those whose spectrum is relatively broad (comparable with the width of plateau of the diffraction curve but not broader than the dispersion curve itself). Then after the propagation in the SC the beam is not filtered (all spectral components are allowed to propagate), however the high spatial components acquire a nonparabolic phase shift. Afterward in the free propagation behind the SC, this phase shift cannot be more compensated.

In this way the model B states that the beam is focused at the same distance as follows from model A, however the width at the waist is no more the same as at the incident in the SC (as predicted by model A) but is affected due to aberrations [Fig. 2(b)]. In general the width is increased. The evaluation of the width at the waist can be performed considering that the width of the parabolic part of the dispersion curve is approximately equal to the width of the loop of dispersion curve. As the spectral width is roughly $\Delta k_f=\Delta\Omega/2$ it follows that

$$\Delta x_f=4/\Delta\Omega. \tag{6}$$

In Fig. 3(b) the beamwidth, evaluated numerically as the width at half of the maximum amplitude in focus, is depicted

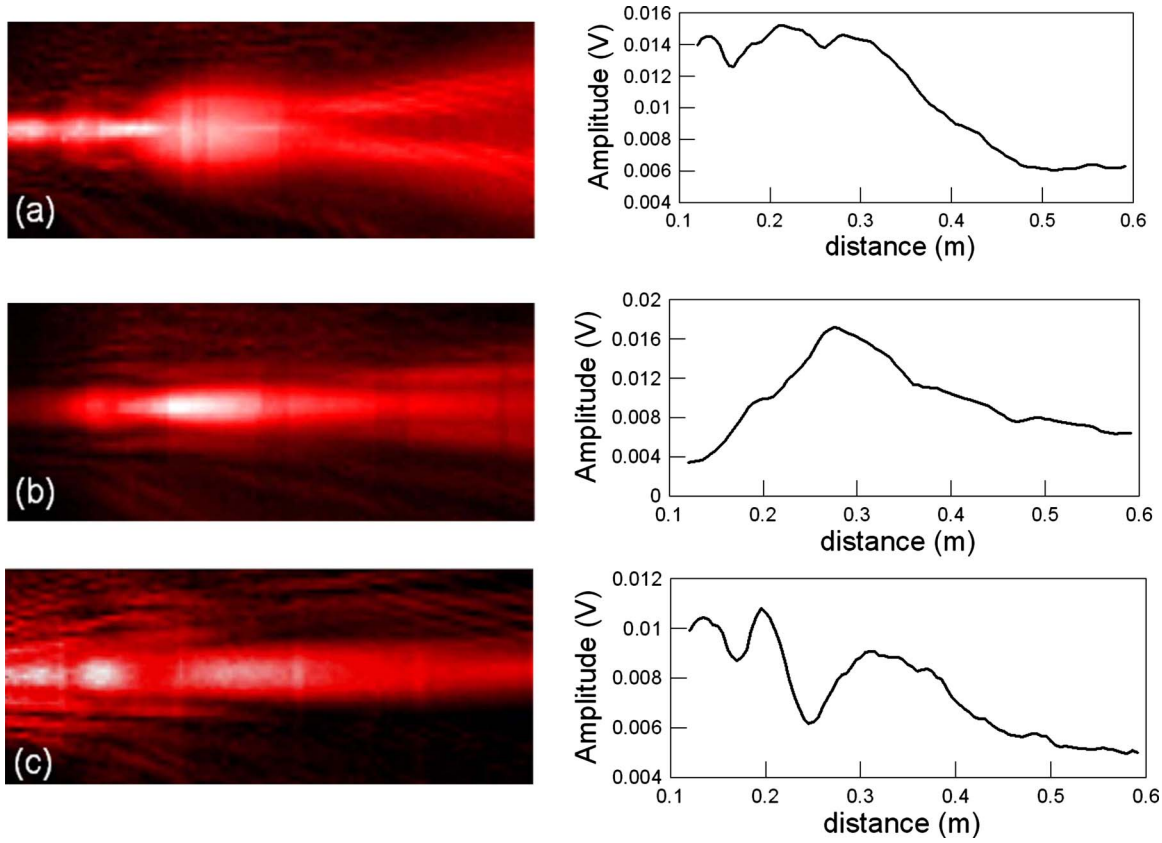

FIG. 4. (Color online) Experimental results for (a) 225 kHz, (b) 240 kHz, and (c) 255 kHz. The left column shows the spatial distribution (in false color) in the *XZ* plane. The spatial dimensions are 20×50 cm^2. The right column shows the measured amplitude distribution along the z axis.

together with the analytical prediction Eq. (6). Note that, due to the normalizations used, the width in the real space is scaled by a factor $a/2\pi$.

(3) Model C. This model considers that not only the phase of the beam (in the spatial spectrum domain) is distorted but also its amplitude. Some spatial spectrum components are removed (filtered out) corresponding to the angular band gap [region d in Fig. 1(b)]. This results in a complicated waist around the focal point.

The spectrum is filtered at around the cross points of the dispersion circles of the harmonic components. A simple geometrical analysis shows that these points are located at $K_f=\pm\Delta\Omega/2$. The beam after crossing the crystal now consists of two parts: a part containing the central region of the spectrum, which behaves in propagation as described by model B and two sidelobes containing the high unfiltered spatial frequencies, those with $|K|>K_f$. The resulting field distribution is even more strongly distorted at the beam waist than predicted by the model B. Characteristic is that the beam waist makes several periods of oscillations, related with the spatial beat between the central spectral component and the sidebands. As a result, the beam distribution presents a modulated profile where several focuses are apparent, as observed in Fig. 2(c), and also in the experimental measurements of the next section.

IV. EXPERIMENT

The results of the preceding section have been checked experimentally in the case of a narrow beam, excited by a piezoelectric transducer. The emitted beam had a frequency-dependent half width covering three to four lattice periods. The experimental setup is basically the same used in Ref. 5 to demonstrate the self-collimation phenomenon of ultrasonic beams, which we summarize for convenience. The sonic crystal used in the experiments was designed according the parameters described above, total length of the crystal being $L=10$ cm. The crystal was immersed in a Plexiglas tank, with dimensions $1\times 1\times 2$ m^3, filled with water, which acted as a host medium. A narrow ultrasonic source with radius $R=1.25$ cm was placed 5 mm close to one of the flat boundaries of the crystal (entrance plane) oriented in the $\langle 100\rangle$ direction and the pressure distribution was measured with a needle hydrophone. The source radiates a nearly Gaussian ultrasonic beam (with an effective width approximately half than that of the source) with measurable amplitude in the frequency interval ranging from 150 to 260 kHz, which covers most of the frequencies of interest in the second propagation band, where the experiments were performed. All the signal generation and acquisition process is based on a National Instruments PXI-technology controller NI8176, which also controls an OWIS GmbH two-axis mo-

torized system that allows the hydrophone to scan the pressure distribution along the whole space beyond the exit plane of the crystal, for a given frequency component.

In order to visualize the beam propagation after the crystal and the focusing effect, in Fig. 4 we show the experimental measurements along the *XZ* plane (left column) and the amplitude distribution along the axis (right column) for three different frequencies. The experimental results show some unique features in the spatial distribution of the beams after crossing the crystal, already anticipated by the theoretical analysis. At low frequencies, close to the self-collimation point [Fig. 4(a)] is apparent a strong distortion of the beam in the neighborhood of the focal region, located close to the exit plane. In fact, a focal distance cannot be unambiguously defined. Also typical for narrow beams in the low-frequency regime is a spatial separation of the pressure distribution into two lobes in the far field. Measured distribution is in accordance with the results of the numerical simulation shown in Fig. 2(c), performed for similar parameters.

At intermediate frequencies a clean, lenslike profile is formed, with a well-defined maximum corresponding to the focal point, as shown in Fig. 4(b). At higher frequencies, approaching the band edge, several focuses (field maxima) are observed. The point with maximum pressure is located at a fixed (frequency-independent) position, close to the crystal but the true (dynamic) focus corresponds to the last maximum (that located more far away from the SC). The existence of the spatial beatings can be attributed to the spatial filtering effect described in Fig. 1(b) and in model C presented in Sec. III.

In Fig. 5 position of the focus as evaluated from numerical simulation (open circles) is compared with the experimentally measured values (black circles), for frequencies in the second propagation band ranging from 230 to 260 kHz. In this band, the middle of the bang gap is located at 280 kHz and focal distance cannot be measured for frequencies higher than 260 kHz because strong uncertainty (as is apparent in the error bars in Fig. 5). We expect, according to the model, that the focal distance increases monotonically when the source frequency approaches the band edge, with a corresponding decrease in amplitude.

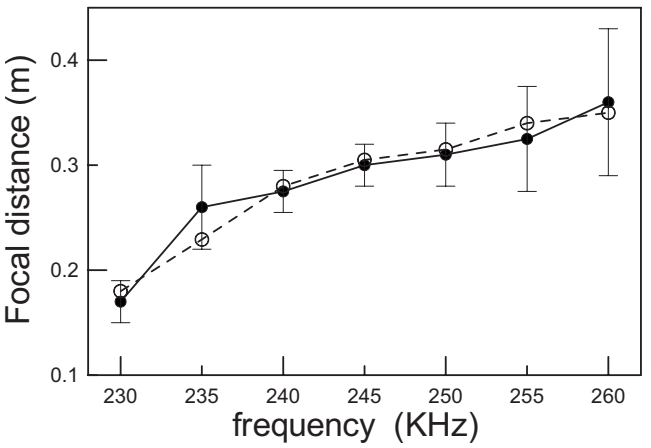

FIG. 5. Focal distance for a narrow beam, as obtained numerically and experimentally. Open symbols: numerics and full symbols: experiment.

V. CONCLUSIONS

The propagation characteristics, and, in particular, the focusing effect, of acoustic beams after crossing a SC have been studied both theoretically and experimentally. The field distribution is shown to depend strongly on the beam size and frequency, and different models for broad, intermediate, and narrow beams are proposed in the framework on the paraxial approximation. Explicit formulas for the focal distance and the beamwidth at the waist are proposed.

It is shown that, in the case of a narrow beam (covering few crystal periods) with a correspondingly broad spatial spectrum, the crystal can result in a strong distortion of the beam profile at particular frequencies, as a consequence of spatial filtering effects (modification of the spatial spectrum of the incident beam) related to the particular form of the dispersion surfaces. A dependence of the focal distance with the frequency is also predicted and experimentally verified in the case of narrow beams with good agreement.

ACKNOWLEDGMENTS

This work was financially supported by the Spanish Ministerio de Ciencia e Innovación and the European Union FEDER through Projects No. FIS2008-06024-C03 and No. FIS2008-06024-C02.

[1] J. D. Joannopoulos, S. G. Johnson, J. N. Winn, and R. D. Meade, *Photonic Crystals: Molding the Flow of Light* (Princeton University Press, Princeton, NJ, 2008).
[2] A. Khelif, B. Aoubiza, S. Mohammadi, A. Adibi, and V. Laude, Phys. Rev. E **74**, 046610 (2006).
[3] H. Kosaka, T. Kawashima, A. Tomita, M. Notomi, T. Tamamura, T. Sato, and S. Kawakami, Phys. Rev. B **58**, R10096 (1998).
[4] I. Pérez-Arjona, V. J. Sánchez-Morcillo, J. Redondo, V. Espinosa, and K. Staliunas, Phys. Rev. B **75**, 014304 (2007).
[5] V. Espinosa, V. J. Sánchez-Morcillo, K. Staliunas, I. Pérez-Arjona, and J. Redondo, Phys. Rev. B **76**, 140302(R) (2007).
[6] C. Luo, S. G. Johnson, J. D. Joannopoulos, and J. B. Pendry, Phys. Rev. B **68**, 045115 (2003).
[7] V. Laude, D. Gérard, N. Khelfaoui, C. F. Jerez-Hanckes, S. Benchabane, and A. Khelif, Appl. Phys. Lett. **92**, 094104 (2008).
[8] M.-H. Lu, C. Zhang, L. Feng, J. Zhao, Y.-F. Chen, Y.-W. Mao, J. Zi, Y.-Y. Zhu, S.-N. Zhu, and N.-B. Ming, Nature Mater. **6**, 744 (2007).
[9] L. Feng, X.-P. Liu, M.-H. Lu, Y.-B. Chen, Y.-F. Chen, Y.-W. Mao, J. Zi, Y.-Y. Zhu, S.-N. Zhu, and N.-B. Ming, Phys. Rev. Lett. **96**, 014301 (2006).
[10] L. Feng, X.-P. Liu, Y.-B. Chen, Z.-P. Huang, Y.-W. Mao, Y.-F. Chen, J. Zi, and Y.-Y. Zhu, Phys. Rev. B **72**, 033108 (2005).

[11] B. C. Gupta and Z. Ye, Phys. Rev. E **67**, 036603 (2003).
[12] C. H. Kuo and Z. Ye, J. Phys. D **37**, 2155 (2004).
[13] L. S. Chen, C. H. Kuo, and Z. Ye, Appl. Phys. Lett. **85**, 1072 (2004).
[14] C. Qiu, X. D. Zhang, and Z. Y. Liu, Phys. Rev. B **71**, 054302 (2005).
[15] M. Ke, Z. Y. Liu, C. Y. Qiu, W. Wang, J. Shi, W. Wen, and P. Sheng, Phys. Rev. B **72**, 064306 (2005).
[16] A. Sukhovich, L. Jing, and J. H. Page, Phys. Rev. B **77**, 014301 (2008).
[17] S. X. Yang, J. H. Page, Z. Y. Liu, M. L. Cowan, C. T. Chan, and P. Sheng, Phys. Rev. Lett. **93**, 024301 (2004).